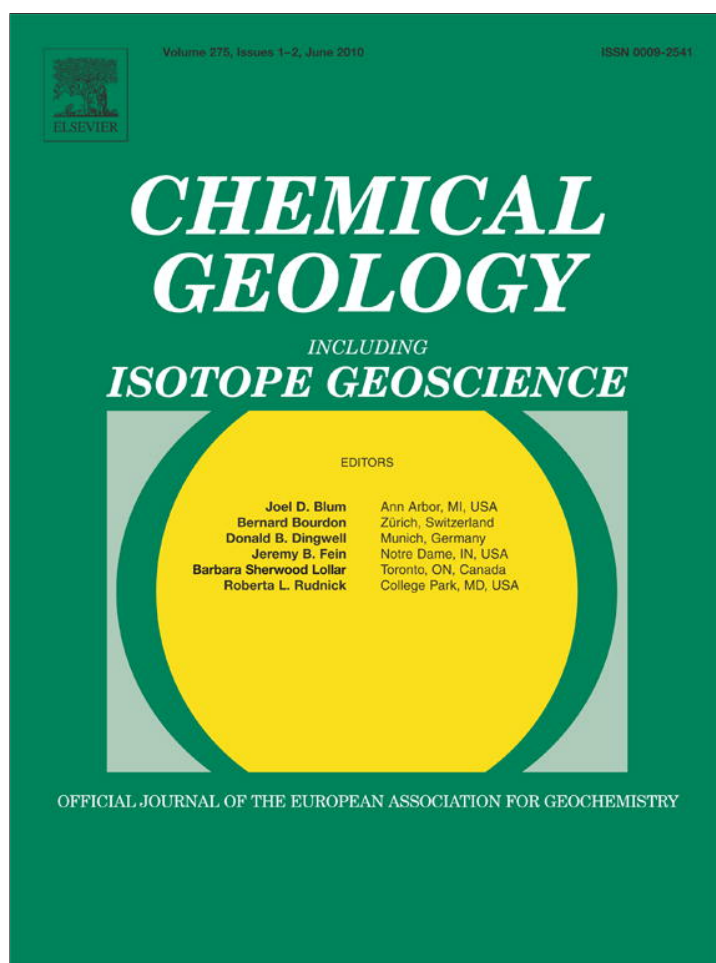


Provided for non-commercial research and education use.
Not for reproduction, distribution or commercial use.



This article appeared in a journal published by Elsevier. The attached copy is furnished to the author for internal non-commercial research and education use, including for instruction at the authors institution and sharing with colleagues.

Other uses, including reproduction and distribution, or selling or licensing copies, or posting to personal, institutional or third party websites are prohibited.

In most cases authors are permitted to post their version of the article (e.g. in Word or Tex form) to their personal website or institutional repository. Authors requiring further information regarding Elsevier's archiving and manuscript policies are encouraged to visit:

<http://www.elsevier.com/copyright>



Contents lists available at ScienceDirect

Chemical Geology

journal homepage: www.elsevier.com/locate/chemgeo

Raman spectra of ice and salt hydrates in synthetic fluid inclusions

Miriam Baumgartner, Ronald J. Bakker*

Department of Applied Geosciences and Geophysics, Mineralogy and Petrology, University of Leoben, Leoben, Austria

ARTICLE INFO

Article history:

Received 24 February 2010

Received in revised form 25 April 2010

Accepted 26 April 2010

Editor: J. Fein

Keywords:

Salt hydrates

Ice

Fluid inclusions

Raman spectroscopy

ABSTRACT

Raman spectra of ice, $\text{NaCl}\cdot 2\text{H}_2\text{O}$ (hydrohalite), $\text{CaCl}_2\cdot 6\text{H}_2\text{O}$ (antarcticite), $\alpha\text{-CaCl}_2\cdot 4\text{H}_2\text{O}$, $\gamma\text{-CaCl}_2\cdot 4\text{H}_2\text{O}$, $\text{CaCl}_2\cdot 2\text{H}_2\text{O}$ (sinjarite), $\text{MgCl}_2\cdot 12\text{H}_2\text{O}$, $\text{FeCl}_2\cdot 6\text{H}_2\text{O}$, $\text{FeCl}_2\cdot 4\text{H}_2\text{O}$, and a LiCl hydrate are characterized in synthetic fluid inclusions in quartz at about -190°C . Each hydrate can be distinguished on its characteristic Raman bands, which occur at wavenumbers in the range of the stretching vibration mode of water (2800 to 4000 cm^{-1}). The spectra provide the basis for the interpretation of Raman spectra obtained in natural fluid inclusions.

© 2010 Elsevier B.V. All rights reserved.

1. Introduction

Salt-bearing aqueous fluid inclusions are common in a variety of geological environments (e.g. Roedder, 1984; Yardley and Graham, 2002). NaCl is the most common salt component within inclusions, which can be only identified directly by destructive methods such as ion chromatography of crushed samples (e.g. Banks and Yardley, 1992) or laser ablation inductively-coupled-plasma mass spectroscopy (e.g. Heinrich et al. 2003). Ice melting temperatures obtained from microthermometry can be directly related to a salt component and can be recalculated as a concentration by using the term of equivalent mass% NaCl (in literature the term *weight%* is often incorrectly used, because weight is a force; see also Bakker, 2004). The presence of cubic crystals in fluid inclusions that readily dissolve at higher temperatures (up to 800°C) is also indicative for the presence of NaCl. However, most types of salts show a similar morphology and the ice melting temperatures below 0°C may result from a large variety of salt types. Consequently, optical microscopy and microthermometry are inconclusive methods for identifying the type of salt component, which is dissolved in the aqueous solution or present as cubic crystals. Eutectic reactions observed during microthermometric analysis of fluid inclusions are generally used to identify the salt system in fluid inclusion research (e.g. Borisenko, 1977). However, due to metastability resulted from inhibition of salt hydrate or ice nucleation and poor microscopical resolution, those reactions are often absent or difficult to observe

(Bakker, 2004; Baumgartner and Bakker, 2009). Therefore, optical investigations are often not sufficient for understanding the complexity of phase equilibria at low temperatures in salt-bearing aqueous fluid inclusions. At low temperatures, water in the presence of dissolved salts form salt hydrates (e.g. $\text{NaCl}\cdot 2\text{H}_2\text{O}$) with a well-defined number of H_2O molecules in the crystal lattice (e.g. Franks, 1972, 1973). In Raman spectroscopic analyses, those molecules have a limited amount of vibrational modes, which are most prominent at wavenumbers in the stretching region of water, between 2800 and 4000 cm^{-1} (O–H vibrations). Therefore, the stretching region of water is the most informative region for identifying the phases occurring in aqueous fluid inclusions, i.e. liquid, ice, and salt hydrates. The Raman bands are characteristic for each specific salt hydrate and can be used to identify the type of dissolved salt from specific hydrate phases (Dubessy et al., 1982; Dubessy et al., 1992; Bakker, 2004). The available Raman spectroscopic data of salt hydrates are limited and partly inconsistent. This study gives a summary and comparison of existing data and presents as well new datasets. Reference Raman spectra of ice and salt hydrates, i.e. $\text{NaCl}\cdot 2\text{H}_2\text{O}$ (hydrohalite), $\text{CaCl}_2\cdot 6\text{H}_2\text{O}$ (antarcticite), $\alpha\text{-CaCl}_2\cdot 4\text{H}_2\text{O}$, $\gamma\text{-CaCl}_2\cdot 4\text{H}_2\text{O}$; $\text{CaCl}_2\cdot 2\text{H}_2\text{O}$ (sinjarite), $\text{MgCl}_2\cdot 12\text{H}_2\text{O}$, $\text{FeCl}_2\cdot 6\text{H}_2\text{O}$, $\text{FeCl}_2\cdot 4\text{H}_2\text{O}$ and a LiCl-hydrate, which nucleated during freezing experiments in the synthetic fluid inclusions in quartz were obtained. Those spectra can be used for the identification of salt hydrates in natural fluid inclusions, which may nucleate during microthermometric investigations.

2. Methods

Fluid inclusions have been synthesized in thermal cracked natural quartz cores (see Baumgartner, 2009). These experiments were

* Corresponding author. Department of Applied Geosciences, Mineralogy and Petrology, University of Leoben, Peter-Tunner Str. 5, A-8700 Leoben, Austria. Tel.: +43 3842 402 6211; fax: +43 3842 47016.

E-mail address: bakker@unileoben.ac (R.J. Bakker).

performed with the pure water system and binary salt-water systems of NaCl–H₂O, CaCl₂–H₂O, MgCl₂–H₂O, FeCl₂–H₂O, and LiCl–H₂O. Microthermometry was performed with a LINKAM MDS 600 heating–freezing stage and samples were cooled by liquid nitrogen to –190 °C. The stage was calibrated with synthetic fluid inclusions of CO₂ (melting at –56.6 °C) and H₂O (melting at 0.0 °C and critical homogenisation at 374 °C). The analytical error of temperature measurements is about 0.2 °C. Raman spectra of salt hydrates at low temperatures were recorded by attaching the heating–freezing stage to the Raman spectrometer. Identification of solid species was performed with a LABRAM (ISA Jobin Yvon) instrument using a frequency-doubled 120 mW polarized Nd-YAG laser with an excitation wavelength of 532.2 nm. All measurements were taken with an LMPlan FI 100×/0.80 n.a. objective lens (Olympus). The power of the laser at the quartz sample is about 1 to 1.5 mW. Raman spectra were taken in the range 2800 to 4000 cm^{–1}, where the most characteristic O–H vibrational modes of all salt hydrates occur. The pixel-resolution of the Peltier-cooled CCD detector (1024×256 pixel, open electrode chip) is about 1.0 to 1.2 cm^{–1}. The wavenumbers are calibrated with the Rayleigh scattering (0 cm^{–1}), silicon (520.7 cm^{–1}), and polyethylene (main peaks at 1062.1, 1128.09, 1294.8, 1438.8, 2847.8, and 2880.9 cm^{–1}), by defining corrected wavenumbers in a linear best-fit equation of measured wavenumbers. During heating and freezing of the synthesized inclusions, hydrates nucleate and Raman spectra of these hydrates were collected subsequently at various temperatures. The integration time varied between 10 and 300 s, depending on the signal intensity of the inclusions, the volume of the inclusions, the volume of the hydrate crystals, and the depth of the inclusions in the host quartz. Each spectrum is obtained with 4 accumulations.

3. Raman spectra of ice and salt hydrates

3.1. Ice

The Raman spectrum of water is a relative weak signal in the range 2800 to 4000 cm^{–1} at room temperature. The presence of an aqueous liquid solution in fluid inclusions hosted in minerals, which reveal a relatively high background signal (e.g. calcite, fluorite), may not be detectable by Raman spectroscopy. This study has revealed that ice has a pronounced spectrum at low temperature and can be even detected in host crystals, which show fluorescence. Raman measurements on synthetic fluid inclusions in quartz reveal main peak positions for ice at about 3090 ± 3 cm^{–1} at –190 °C (Fig. 1). Additionally, a broad band can be defined at 3218 cm^{–1} and at approximately 3321 cm^{–1}. The measured fluid inclusion in Fig. 1 has a critical density, and upon freezing a vapour phase remains present. Inclusions containing all liquid, i.e. absence of the vapour bubble, reveal a different spectrum after the nucleation of ice: at –190 °C the main peak occurs at lower relative wavenumbers than the previously mentioned number, such as the 3073 cm^{–1} shown in Fig. 2. Freezing of these inclusions cannot be optically identified, but the Raman spectrum that is typically for a liquid H₂O solution was not detected in frozen “all-liquid” inclusions, indicating that all water was transformed into ice. Relative wavenumbers down to about 3050 cm^{–1} were observed in other “all-liquid” inclusions. This shift in relative wavenumbers is reproducible in the same fluid inclusion, indicating that inclusions do not re-equilibrate or decrepitate. The small inclusion in Fig. 2 was subsequently heated to –5 °C in order to recrystallise the ice and cooled again down to –190 °C. The ice peak was now shifted to 3096 cm^{–1}, at a significantly higher value than the peak position illustrated in Fig. 1. The shift in relative wavenumbers due to this recrystallisation process is also reproducible.

Fluid inclusions are regarded as containers with a constant total volume, therefore, ice nucleation must result in high internal pressures, due to the differences in the molar volume of ice and water. Garg (1988) reported a peak-shift to lower wavenumbers as a

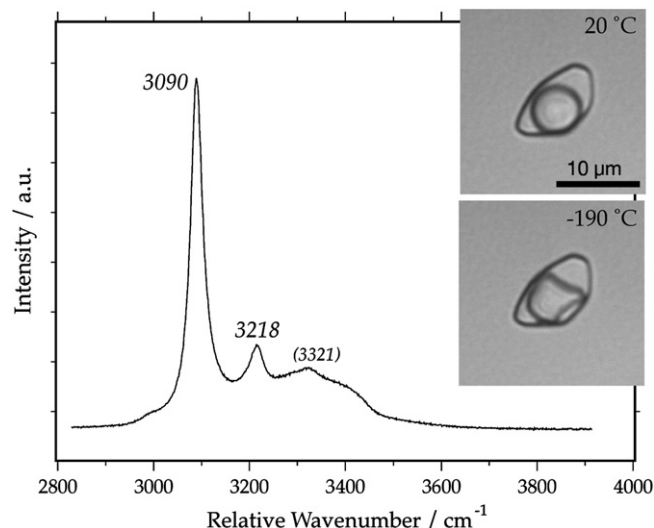


Fig. 1. Raman spectrum of ice at –190 °C. The measured fluid inclusion contains vapour and water at 20 °C (with a critical density), and vapour and ice at –190 °C.

function of pressure. He observed the main peak positions for ice at –185.5 °C at 3088 cm^{–1} at 0.0001 GPa, whereas at 0.353 GPa the peak shifts to 3034 cm^{–1}. In the present study, a linear best-fit equation through his dataset reveals the pressure as a function of the peak shift:

$$p = 19.226 - 0.0062249 \cdot \Delta\nu_1 \quad (1)$$

where p is pressure in GPa and $\Delta\nu_1$ is the relative wavenumber of the main ice peak obtained by Raman spectroscopy (in cm^{–1}). According to Eq. (1) the observed peak position at 3050 cm^{–1} corresponds to a calculated internal pressure of 240 MPa, whereas the example illustrated in Fig. 2 has an internal pressure of 97 MPa after ice nucleation. After recrystallising the ice at –5 °C, the main ice peak at about –190 °C shifts to higher relative wavenumbers, even exceeding

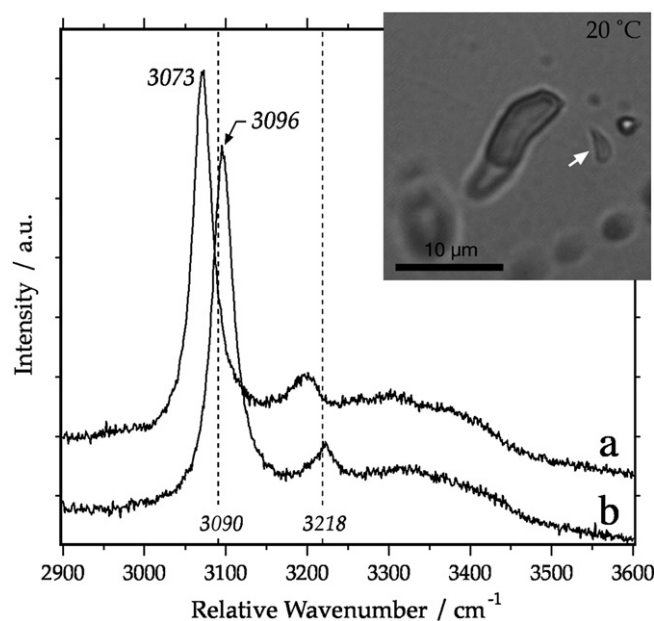


Fig. 2. Raman spectra of ice at –190 °C measured in an “all liquid” fluid inclusion (arrow). a. the spectrum directly measured after the nucleation of ice (main peak at 3073 cm^{–1}); b. the spectrum after recrystallization at –5 °C and recooled to –190 °C (main peak 3096 cm^{–1}). The dashed lines indicate the position of the main peaks as illustrated in Fig. 1.

those values illustrated in Fig. 1, likely due to relaxation processes (e.g. elasticity) in the quartz adjacent to the overpressurized fluid inclusion. Nevertheless, the fluid inclusions do not reveal any permanent re-equilibration textures, and repeatedly microthermometrical experiments on the same inclusion result in the same shift of relative wavenumbers of the main ice peak.

Dubessy et al. (1982) observed the main ice peak at 3090 cm^{-1} and a minor peak at 3250 cm^{-1} at $-170\text{ }^\circ\text{C}$ in frozen aqueous solutions. Ni et al. (2006) determined the main ice peak at 3098 cm^{-1} in synthetic fluid inclusions at $-180\text{ }^\circ\text{C}$, which significantly differ from this study. Bakker (2004) has quantified the shift in the main peak position of ice as a function of temperature, and has calculated its value at 3102 cm^{-1} at $-190\text{ }^\circ\text{C}$ and at 3105 cm^{-1} at $-170\text{ }^\circ\text{C}$. These numbers also deviate from the values obtained in the present study. Re-examination of the raw data from Bakker (2004) demonstrates differences in the calibration method of wavenumbers. A polynomial best-fit of the second order through the wavenumbers of standards (silicon and polyethylene) results in overestimated wavenumbers above 3000 cm^{-1} . The temperature dependent equation for the main ice peak given by Bakker (2004) has to be adjusted according to the calibration method of this study (Eq. (2)):

$$\Delta\nu_1 = 3082.3 + 0.05498 \cdot T + 0.00051841 \cdot T^2 \quad (2)$$

where T is temperature (in K). A linear combination of Eqs. (1) and (2) results in a definition of the relative wavenumber of the main peak of ice as a function of temperature and pressure:

$$\Delta\nu_1 = 3082.3 + 0.05498 \cdot T + 0.00051841 \cdot T^2 - 160.645 \cdot p \quad (3)$$

where T is temperature (in K), and p is pressure in GPa.

3.2. NaCl hydrates

Hydrohalite can be identified at low temperatures by specific Raman bands, which occur in the OH stretching region of water. In this study, the spectra reveal four main peaks for hydrohalite centred at about $3402 \pm 2\text{ cm}^{-1}$, $3418 \pm 1\text{ cm}^{-1}$, $3432 \pm 2\text{ cm}^{-1}$ and $3536 \pm 4\text{ cm}^{-1}$ at $-190\text{ }^\circ\text{C}$ (see Fig. 3). In addition, two peaks with relatively low amplitude intensities are located at about $3300 \pm 1\text{ cm}^{-1}$ and $3321 \pm 2\text{ cm}^{-1}$. Raman spectra recorded on differently orientated hydrohalite crystals show a variation in relative peak intensities, which is a consequence of the relative crystal orientation compared to the polarized laser beam (compare Fig. 3a and b, Table 1). Temperature changes have only minor influence on the position of the four main peaks. For example, the main peak varies only between 3419 cm^{-1} and 3420 cm^{-1} between $-190\text{ }^\circ\text{C}$ and $-50\text{ }^\circ\text{C}$. At higher temperatures, the Raman bands of hydrohalite are broadening and individual peaks merge into a broader band (see also Bakker, 2004).

Previous Raman spectroscopic studies on frozen NaCl-bearing aqueous solutions (Dubessy et al., 1982) reveal slightly higher peak positions for hydrohalite, at 3406 , 3422 , 3438 and 3536 cm^{-1} at $-170\text{ }^\circ\text{C}$, whereas the peaks identified at 3089 and 3209 cm^{-1} represent ice (c.f. Fig. 1). The peak values recorded by Samson and Walker (2000) at $-185\text{ }^\circ\text{C}$ in aqueous solutions correspond to the values obtained in this study, i.e. from measurements on single hydrohalite crystals in synthetic fluid inclusions. The Raman bands measured in synthetic inclusions given by Ni et al. (2006) are at significant higher wavenumbers (approximately $+5\text{ cm}^{-1}$) than the values obtained in this study. Bakker (2004) defined five peak positions for hydrohalite at 3326 cm^{-1} , 3407 cm^{-1} , 3424 cm^{-1} , 3439 cm^{-1} and 3539 cm^{-1} by analysing the spectra with Gaussian-Lorentzian contributions, which are also centred at higher wavenumbers compared to the results in this study. Due to improved calibration procedures that are illustrated in the previous paragraph, these values have to be shifted about 6 cm^{-1} to lower wavenumbers.

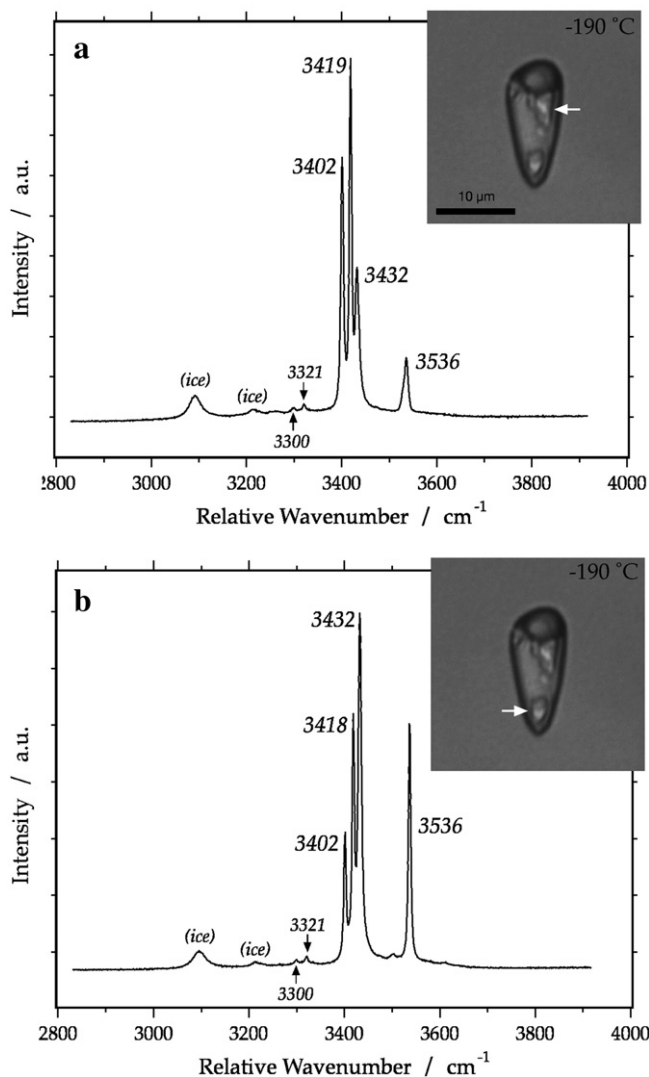


Fig. 3. Raman spectra of hydrohalite at $-190\text{ }^\circ\text{C}$, obtained from two single hydrate crystal with different orientations, as illustrated in the synthetic fluid inclusion (arrows). The relative intensities of spectra a and b are given in Table 1.

3.3. CaCl₂ hydrates

Cooling experiments with inclusions containing a fluid in the $\text{CaCl}_2\text{-H}_2\text{O}$ system may lead to the precipitation of various stable and metastable solid phases (see Baumgartner and Bakker, 2009). High saline inclusions (about 50 mass% CaCl_2) may nucleate different CaCl_2 -hydrates, i.e. $\text{CaCl}_2 \cdot 6\text{H}_2\text{O}$ (antarcticite), $\alpha\text{-CaCl}_2 \cdot 4\text{H}_2\text{O}$, $\gamma\text{-CaCl}_2 \cdot 4\text{H}_2\text{O}$, and $\text{CaCl}_2 \cdot 2\text{H}_2\text{O}$ (sinjarite), and these hydrates can be distinguished on their characteristic Raman bands and melting behaviour. Raman spectra of antarcticite obtained from synthesized inclusions, reveal characteristic peak positions in the OH stretching region that differ from hydrohalite (Fig. 4, Table 2). The four main peak positions are

Table 1
Raman peak positions, in relative wavenumbers ($\Delta\nu$) and their relative intensity (maximum 100) of the hydrohalite spectra illustrated in Fig. 3.

$\Delta\nu$ (in cm^{-1})	Rel. int. Fig. 3a	Rel. int. Fig. 3b
3300	2	3
3321	5	3
3402	71	37
3418/3419	100	71
3432	43	100
3536	17	67

centred at 3386 ± 2 , 3405 ± 2 , 3410 ± 2 , and $3430 \pm 1 \text{ cm}^{-1}$ at $-190 \text{ }^\circ\text{C}$ (Fig. 4a). A minor peak is present at $3242 \pm 3 \text{ cm}^{-1}$. The peak with the highest intensity is always located near 3430 cm^{-1} . Depending on the crystallographic orientation, the peaks at 3386, 3405 and 3410 cm^{-1} can merge to a broader band, that is centred on 3405 cm^{-1} (Fig. 4b). The peak centred at 3386 cm^{-1} is only evident as a shoulder in Fig. 4b.

The Raman bands of antarctite in frozen aqueous solutions ($-170 \text{ }^\circ\text{C}$) that were identified by Dubessy et al. (1982) are corresponding only in part to the values obtained in this study. The peak position centred at 3090 cm^{-1} overlap with the main peak position observed of ice (c.f. Fig. 1), and the four main peaks are located at lower values, i.e. approximately 3 wavenumbers, compared to our results. Dubessy et al. (1982) identified two minor peaks at 3448 and 3513 cm^{-1} , which are not detected in the synthetic fluid inclusions. The Raman bands of antarctite given by Samson and Walker (2000) at temperatures between -175 and $-185 \text{ }^\circ\text{C}$ (at 3386, 3406 and 3432 cm^{-1}) correspond to values of our study.

The Raman spectrum obtained from $\alpha\text{-CaCl}_2 \cdot 4\text{H}_2\text{O}$ at $-190 \text{ }^\circ\text{C}$ reveals main peak positions centred at about 3365 ± 6 and $3445 \pm 2 \text{ cm}^{-1}$ (Fig. 5,

Table 2

Raman peak positions, in relative wavenumbers ($\Delta\nu$) and their relative intensity (maximum 100) of the antarctite spectra illustrated in Fig. 4.

$\Delta\nu$ (in cm^{-1})	Rel. int. Fig. 4a	Rel. int. Fig. 4b
3242	2	4
3386	15	–
3404/3405	34	56
3410	40	–
3430/3431	100	100

Table 3). The highest intensity is always obtained from the latter peak, independent of the orientation of the hydrate crystal. Shoulders on the main peak are located at 3423 ± 3 and $3475 \pm 5 \text{ cm}^{-1}$. The peak at 3365 cm^{-1} has a relatively broad width at half height (FWHM), which may have resulted from the overlap of multiple components (i.e. Gaussian-Lorentzian functions). This may also cause the relatively wider span in peak positions dependent on hydrate crystal orientation. A broad double peak is observed in the range 3150 cm^{-1} to 3250 cm^{-1} .

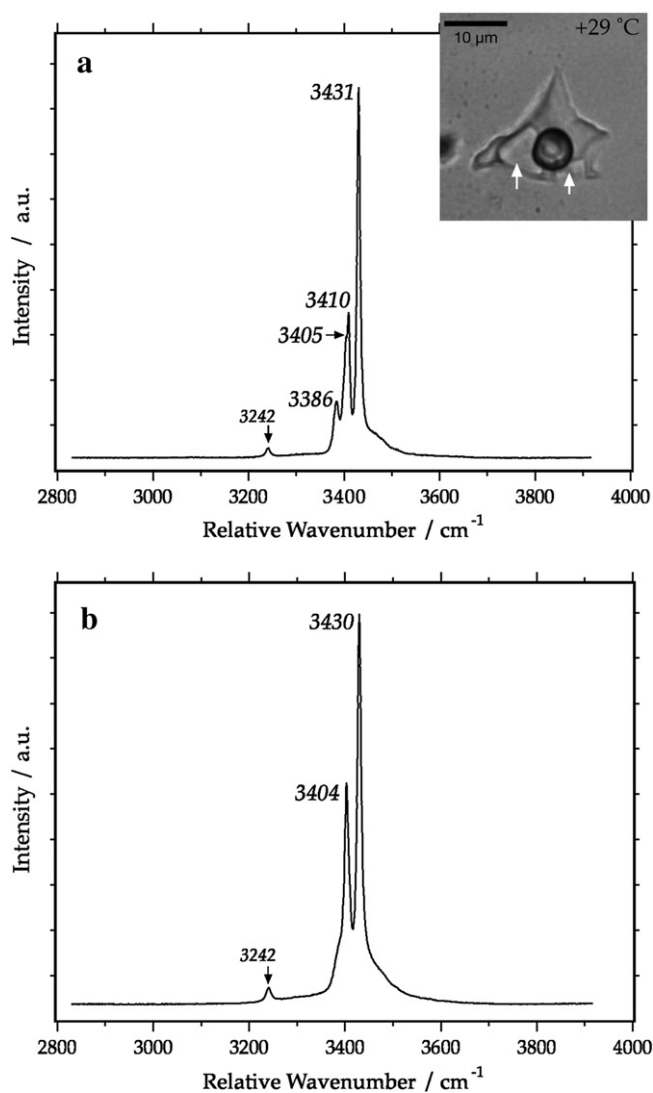


Fig. 4. Raman spectra of antarctite at $-190 \text{ }^\circ\text{C}$. Variable peak intensities (a and b) are caused by different crystallographic orientation of the measured hydrate crystals (see Table 2). The measured fluid inclusion contains at room temperature a metastable phase assemblage of vapour and brine. After cooling and hydrate nucleation, a stable phase assemblage was obtained with brine, vapour and antarctite, which melts at about $30 \text{ }^\circ\text{C}$.

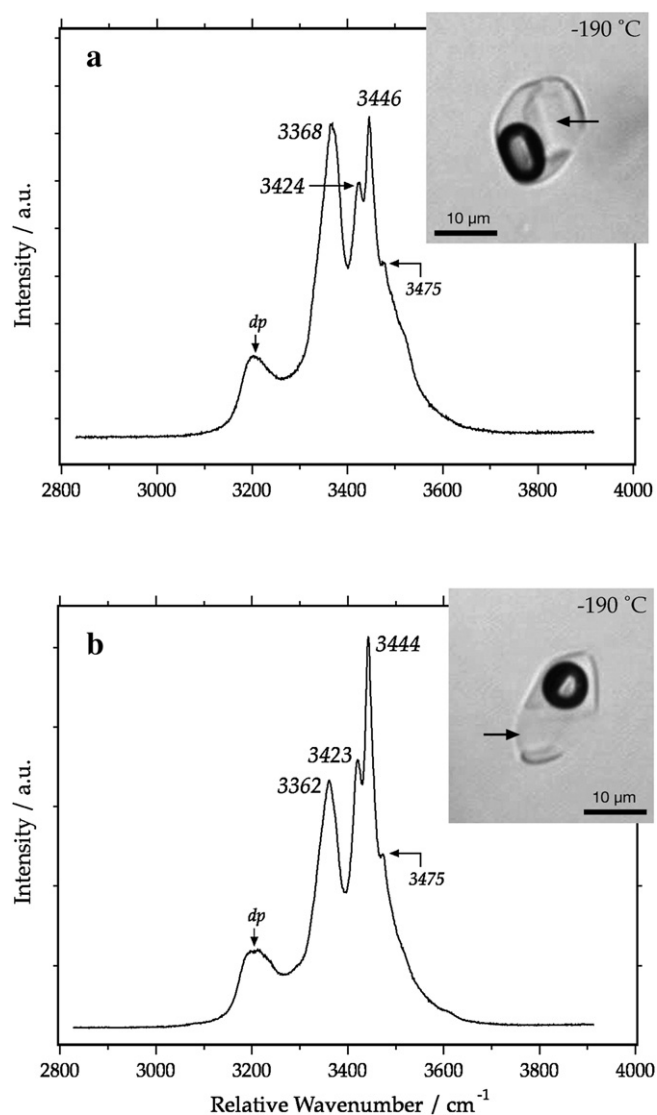


Fig. 5. Raman spectra of $\alpha\text{-CaCl}_2 \cdot 4\text{H}_2\text{O}$ at $-190 \text{ }^\circ\text{C}$. Variable peak intensities (a and b) are caused by different crystallographic orientation of the measured hydrate crystals (see Table 3). *dp* indicates a double peak, that consist of at least two Gaussian-Lorentzian components. The images of the inclusions illustrate metastable phase assemblages at $-190 \text{ }^\circ\text{C}$ (i.e. vapour + brine + hydrate) and the positions of measurement (arrows).

Table 3
Raman peak positions, in relative wavenumbers ($\Delta\nu$) and their relative intensity (maximum 100) of the α - $\text{CaCl}_2 \cdot 4\text{H}_2\text{O}$ spectra illustrated in Fig. 5.

$\Delta\nu$ (in cm^{-1})	Rel. int. Fig. 5a	Rel. int. Fig. 5b
3196/3197	dp (24)	dp (19)
3215/3217		
3362/3368	98	63
3423/3424	78	68
3444/3446	100	100
3475	54	44

Deconvolution of this part of the spectrum resulted in two Gaussian–Lorentzian components centred at approximately 3196 and 3216 cm^{-1} .

γ - $\text{CaCl}_2 \cdot 4\text{H}_2\text{O}$ is defined by a relatively broad signal at -190°C in the range 3100 cm^{-1} to 3600 cm^{-1} (Fig. 6), which implies the presence of a poorly crystallised phase (see also Baumgartner and Bakker, 2009). The highest intensity of this spectrum is obtained at about 3434 cm^{-1} . Shoulders, which may appear due to different orientations of the hydrate crystal, are defined at about 3260, 3392, 3463 and 3575 cm^{-1} .

Sinjarite ($\text{CaCl}_2 \cdot 2\text{H}_2\text{O}$) displays a complex spectrum morphology at -190°C with the main peaks centred at 3424 ± 2 and $3376 \pm$

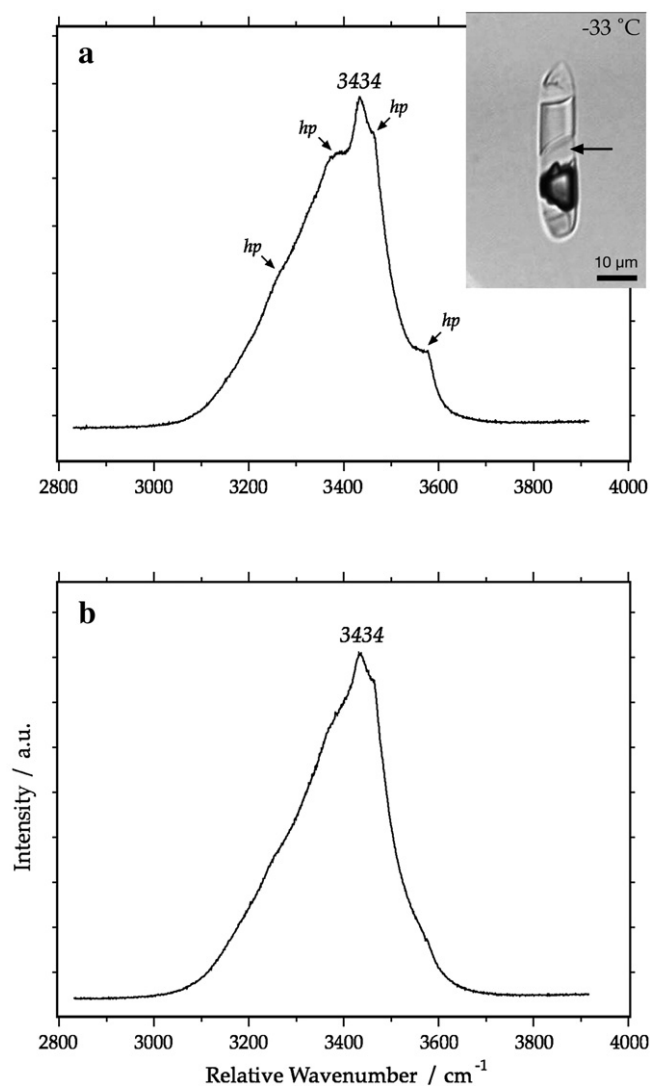


Fig. 6. Raman spectra of γ - $\text{CaCl}_2 \cdot 4\text{H}_2\text{O}$ at -190°C . a and b reveal the variation of the morphology of this broad spectrum caused by different crystallographic orientations. *hp* are hidden peaks that are suspected in the spectrum, and appear as shoulders.

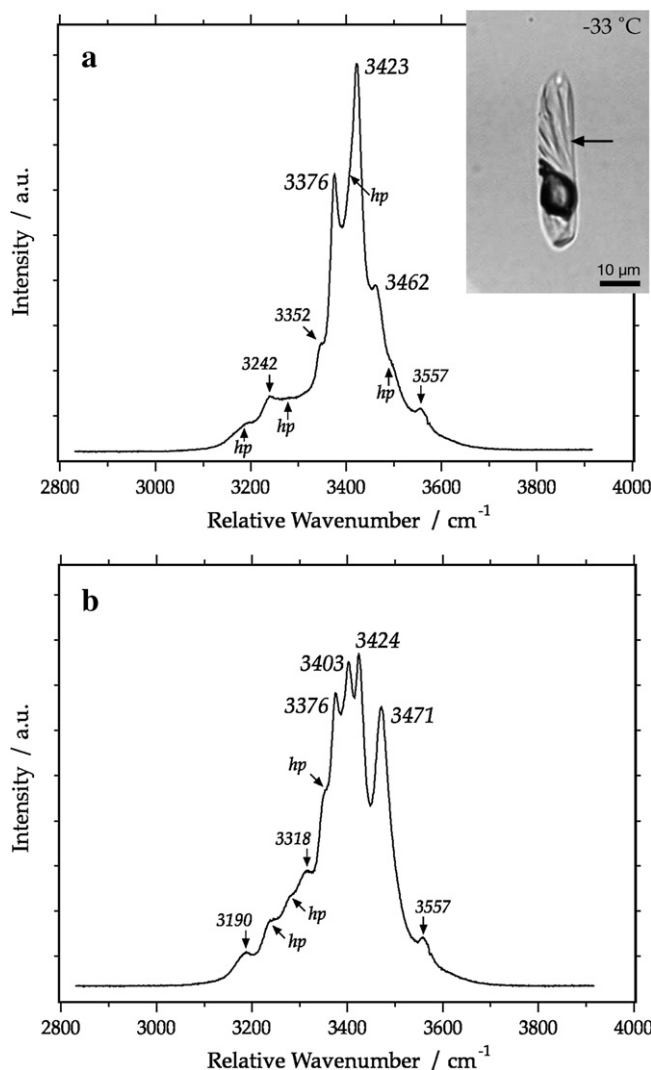


Fig. 7. Raman spectra of sinjarite at -190°C . Variable peak intensities (a and b) are caused by different crystallographic orientation of the measured hydrate crystals (see Table 4). *hp* are hidden peaks that may develop into real peaks in specific orientations, or remain present as shoulders. Note that this fluid inclusion is the same one as illustrated in Fig. 6 (see also Baumgartner and Bakker, 2009).

1 cm^{-1} (Fig. 7, Table 4). Depending on the orientation of the hydrate crystal, a third main peak may occur at $3403 \pm 3 \text{ cm}^{-1}$. A peak with a broad FWHH occurs in the range 3462 to 3471 cm^{-1} . This peak may include multiple Gaussian–Lorentzian components, which are independently varying their intensity with hydrate crystal orientation. Furthermore, shoulders are defined at 3190 ± 2 , 3242 ± 9 , 3285 ± 4 , 3318 ± 5 , 3352 ± 4 and $3557 \pm 2 \text{ cm}^{-1}$. These shoulders may be

Table 4
Raman peak positions, in relative wavenumbers ($\Delta\nu$) and their relative intensity (maximum 100) of the sinjarite spectra illustrated in Fig. 7.

$\Delta\nu$ (in cm^{-1})	Rel. int. Fig. 7a	Rel. int. Fig. 7b
3190	hp	7
3242	13	hp
(3285)	hp	hp
3318	hp	33
3352	26	hp
3376	66	85
3403	hp	94
3423/3424	100	100
3462/3471	43	80
3557	8	13

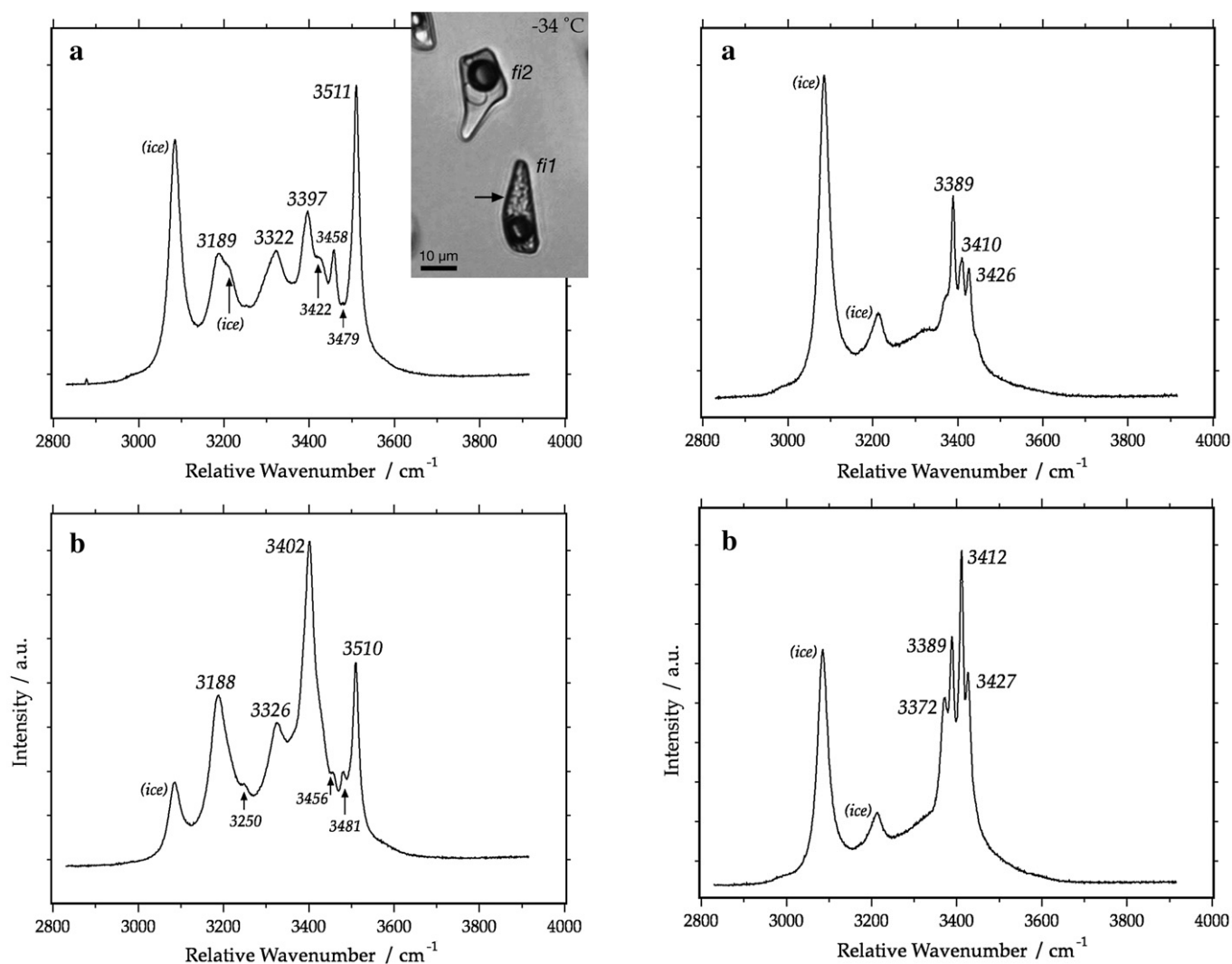


Fig. 8. Raman spectra of $\text{MgCl}_2 \cdot 12\text{H}_2\text{O}$ at -190°C . Variable peak intensities (a and b) are caused by different crystallographic orientation of the measured hydrate crystals (see Table 5). The illustrated fluid inclusions contain a stable phase assemblage (*fi1*: ice + hydrate + vapour) and a metastable phase assemblages (*fi2*: ice + brine + vapour) and at -34°C . The arrow indicates the position of the laser-spot during the measurement.

hidden or camouflaged by main peaks depending on hydrate crystal orientation.

3.4. MgCl_2 hydrate

MgCl_2 -hydrate and ice nucleation may occur during cooling experiments in synthetic fluid inclusions that contain a H_2O - MgCl_2 solution. Fluid composition with less than 40 mass% MgCl_2 may nucleate

Table 5

Raman peak positions, in relative wavenumbers ($\Delta\nu$) and their relative intensity (maximum 100) of the $\text{MgCl}_2 \cdot 12\text{H}_2\text{O}$ spectra illustrated in Fig. 8.

$\Delta\nu$ (in cm^{-1})	Rel. int. Fig. 8a	Rel. int. Fig. 8b
3188/3189	60	53
3250	–	23
3322/3326	60	43
3397	80	–
3402	–	100
3422	60	–
3456/3458	60	27
3479/3481	35	27
3510/3511	100	60

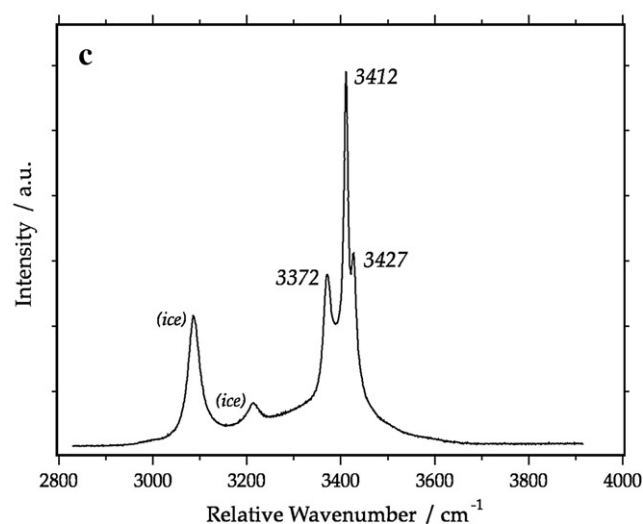


Fig. 9. Raman spectra of $\text{FeCl}_2 \cdot 6\text{H}_2\text{O}$ at -190°C . Variable peak intensities (a, b and c) are caused by different crystallographic orientation of the measured hydrate crystals (see Table 6).

$\text{MgCl}_2 \cdot 12\text{H}_2\text{O}$. The Raman spectrum of $\text{MgCl}_2 \cdot 12\text{H}_2\text{O}$ at -190°C is defined by a great number of peaks in the range of 3000 to 3600 cm^{-1} (Fig. 8, Table 5). The main peak is allocated at $3511 \pm 2\text{ cm}^{-1}$. Due to the effect of the crystallographic orientation of the measured hydrate crystals, the peak at 3402 cm^{-1} may exceed this peak in intensity, and it may hide

or overlap with the peaks centred at 3397 ± 5 and $3422 \pm 5 \text{ cm}^{-1}$ due to its broad *FWHH*. Furthermore, the peak at $3189 \pm 5 \text{ cm}^{-1}$ with a broad *FWHH* is of importance to the characterization of $\text{MgCl}_2 \cdot 12\text{H}_2\text{O}$. This peak nearly overlaps with the smaller peak of ice (c.f. Fig. 1). Some minor peaks are present at 3250 ± 4 , 3457 ± 2 , and $3480 \pm 4 \text{ cm}^{-1}$. The spectra illustrated in Fig. 8 also reveal the Raman bands of ice, i.e. 3090 and 3218 cm^{-1} , because the MgCl_2 hydrate and ice could not be completely separated during the measurements.

Most of the Raman bands for $\text{MgCl}_2 \cdot 12\text{H}_2\text{O}$ in aqueous solution measured by Dubessy et al. (1982) at $-170 \text{ }^\circ\text{C}$ correspond to the peak values obtained in synthetic fluid inclusions in this study. The major peak at 3189 cm^{-1} was not observed in aqueous solutions, and the peak at about 3091 cm^{-1} (see Fig. 4 in Dubessy et al., 1982) probably belongs to ice. Small variances in peak values are due to the differences in measurement conditions, e.g. temperature. The occurrence of the Raman band at about 3250 cm^{-1} is not described in previous studies. The variance in morphology of the Raman spectra of $\text{MgCl}_2 \cdot 12\text{H}_2\text{O}$ due to hydrate crystal orientation was also illustrated by Bakker (2004). The Raman bands identified by Bakker (2004) are about 6 cm^{-1} wavenumbers higher than the bands observed in this study, similar to the misfit of values observed for hydrohalite (see Fig. 3) due to previously described calibration method. The temperature influence on the position of the main peak ($\Delta\nu_{\text{Mg}}$) that is centred at 3511 cm^{-1} at $-190 \text{ }^\circ\text{C}$ is given by the improved equation (c.f. Bakker, 2004):

$$\Delta\nu_{\text{Mg}} = 3513.4 - 0.023424 \cdot T - 0.00010709 \cdot T^2 \quad (4)$$

where T is temperature (in K). This equation illustrates a decrease of about 10 cm^{-1} up to $-30 \text{ }^\circ\text{C}$.

3.5. FeCl_2 hydrates

The nucleation of $\text{FeCl}_2 \cdot 6\text{H}_2\text{O}$ occurs in inclusions containing an aqueous solution with less than 54 mass% FeCl_2 . In this study, Raman spectra taken at $-190 \text{ }^\circ\text{C}$ from inclusions with 36 mass% FeCl_2 reveal a mixture of ice (3090 and 3218 cm^{-1}) and $\text{FeCl}_2 \cdot 6\text{H}_2\text{O}$ crystals (Fig. 9), that consist of four Raman bands centred at 3372 ± 2 , 3389 ± 2 , 3411 ± 2 , and $3426 \pm 2 \text{ cm}^{-1}$. Different crystallographic orientations of the measured hydrate crystals may influence the relative intensities (Table 6) of these peaks. As shown in Fig. 9b and c, the peak at 3372 cm^{-1} is only present as a shoulder in the Raman spectrum shown in Fig. 9a. Furthermore, the peak at 3389 cm^{-1} is not detectable in the Raman spectrum shown in Fig. 9c. In microthermometric experiments, some inclusions nucleated a metastable FeCl_2 -hydrate phase, which is most probably $\text{FeCl}_2 \cdot 4\text{H}_2\text{O}$. According to equilibrium thermodynamics, this phase can only be stable in a 54.0 to 77.9 mass% FeCl_2 solution at low temperatures (Linke, 1958). However, metastabilities similar to those observed with CaCl_2 solutions (see Baumgartner and Bakker, 2009) may occur in these inclusions. The Raman spectrum reveals two main peaks at 3386 and 3404 cm^{-1} at $-190 \text{ }^\circ\text{C}$ (Fig. 10) and is significantly different from the previously mentioned FeCl_2 hydrate. The spectrum also reveals a broad band at about 3170 cm^{-1} , and a minor peak at 3520 cm^{-1} .

Table 6
Raman peak positions, in relative wavenumbers ($\Delta\nu$) and their relative intensity (maximum 100) of the $\text{FeCl}_2 \cdot 6\text{H}_2\text{O}$ spectra illustrated in Fig. 9.

$\Delta\nu$ (in cm^{-1})	Rel. int. Fig. 9a	Rel. int. Fig. 9b	Rel. int. Fig. 9c
3372	hp	54	43
3389	100	73	hp
3410/3412	68	100	100
3426/3427	61	63	50

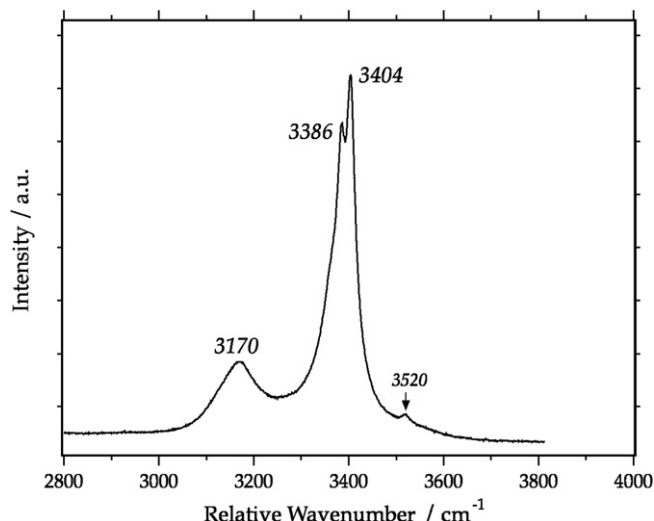


Fig. 10. Raman spectrum of $\text{FeCl}_2 \cdot 4\text{H}_2\text{O}$ at $-190 \text{ }^\circ\text{C}$.

3.6. LiCl hydrate

A Raman spectrum of an unknown hydrate phase of LiCl was obtained in LiCl-bearing aqueous fluid inclusions (Fig. 11). This spectrum is characterized by two band positions centred at 3359 ± 2 and $3376 \pm 1 \text{ cm}^{-1}$ at $-190 \text{ }^\circ\text{C}$. This double peak is modified to a single broad band at $-10 \text{ }^\circ\text{C}$ with the main peak position at 3380 cm^{-1} . Melting temperature of this phase in microthermometric experiments was estimated between 75 and $104 \text{ }^\circ\text{C}$, which reflects the liquidus with $\text{LiCl} \cdot \text{H}_2\text{O}$ (see Baumgartner, 2009).

LiCl hydrate Raman spectra have been reported by e.g. Manewa and Fritz (1972) and Dubessy et al. (1992). Manewa and Fritz (1972) document Raman bands at 3342 , 3434 and 3544 cm^{-1} for $\text{LiCl} \cdot \text{H}_2\text{O}$ and 3445 cm^{-1} for $\text{LiCl} \cdot 2\text{H}_2\text{O}$ at room temperatures, which are significantly different from our results. The Raman band presented by Dubessy et al. (1992) for $\text{LiCl} \cdot 5\text{H}_2\text{O}$ consists of a broad band at approximately 3430 cm^{-1} with a large *FWHH*, and resembles the spectrum of a liquid salt-bearing solution at low temperatures (c.f. Fig. 17 in Bakker, 2004), or a poorly crystallised solid hydrate phase (c.f. Fig. 6). Consequently, the available data on LiCl hydrates are

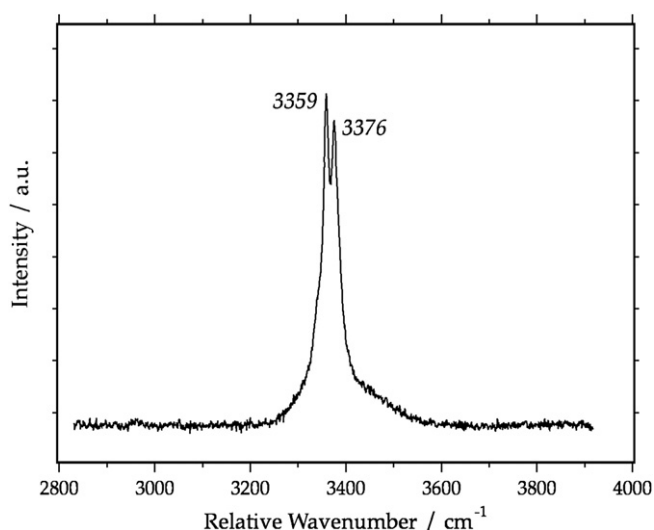


Fig. 11. Raman spectrum of a LiCl hydrate at $-190 \text{ }^\circ\text{C}$.

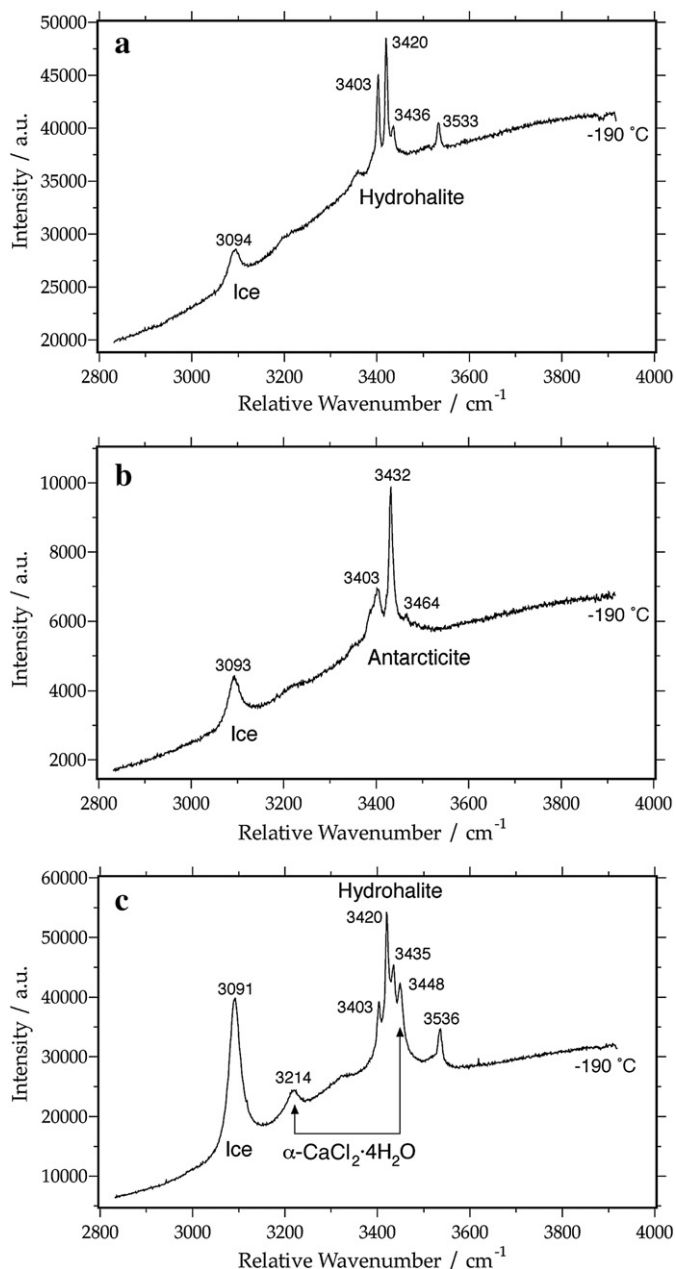


Fig. 12. Raman spectra of natural fluid inclusions in dolomite at -190°C , revealing mixtures of ice and hydrohalite (a), ice and antarctite (b), and ice, hydrohalite and $\alpha\text{-CaCl}_2\cdot 4\text{H}_2\text{O}$ (c). The background signal of the host mineral is relatively high and is increasing in intensity at higher wavenumbers, due to fluorescence using a 532.2 nm wavelength laser source.

inconsistent, and further research is required to identify the specific hydrates.

4. Natural fluid inclusions

Microthermometry is generally used to identify salt components in fluid inclusions by the observation of eutectic temperatures and final melting of ice and salt hydrates (e.g. Borisenko, 1977; Haynes, 1985; Schiffries, 1990; Davis et al., 1990). Multi-component salt systems in natural fluid inclusions show various complex phase assemblages at low temperatures (e.g. Zwart and Touret, 1994; Schiffries, 1990), and an accurate identification by purely optical means is difficult. In combination with microthermometry, Raman spectroscopy at low temperatures in natural fluid inclusions offers the possibility to identify phase assemblages, including specific salt-hydrates, and

thereby the composition of fluid inclusion (see also Bakker, 2004). This combined method have been applied in only a few natural fluid inclusion studies, which reveal simple hydrohalite spectra (e.g. Derome et al., 2007), or complex spectra with a variety of peaks that cannot be assigned to a single hydrate phase (e.g. Gasparrini et al., 2006; Schneider et al., 2008). The supposed Li-rich brines in the Larderello geothermal system (Cathelineau et al., 1994) could not be verified with cryogenic Raman spectroscopy, due to the lack of reference spectra.

Salt-hydrates in a homogeneous assemblage of natural fluid inclusions in dolomite from Carboniferous rocks from the Cantabrian Mountains (see Baumgartner, 2009) were detected with Raman spectroscopy at low temperatures. Mixtures of ice and hydrohalite were detected at -190°C (Fig. 12a, c.f. Figs. 1 and 3) in a variety of inclusions. Other inclusions reveal a mixture of ice and antarctite (Fig. 12b, c.f. Figs. 1 and 4), and occasionally, complex mixtures of ice, hydrohalite, and $\alpha\text{-CaCl}_2\cdot 4\text{H}_2\text{O}$ (Fig. 12c, c.f. Figs. 1, 3, and 5) were identified in the Raman spectra at -190°C . This example illustrates the variety of phase assemblages (and metastabilities) that occur in natural inclusions containing a NaCl–CaCl₂-rich brine. The illustrated spectra in Fig. 12 are mechanical mixtures of ice and hydrate crystals, and are composed of a simple addition of the spectra of individual phases that are present in the inclusion.

5. Conclusions

Cryogenic Raman spectroscopy on synthetic fluid inclusions allows the identification of a variety of salt hydrates that are formed in inclusions from an aqueous liquid solution upon freezing. The selected binary solutions consist of $\text{H}_2\text{O}\text{-NaCl}$, $\text{H}_2\text{O}\text{-CaCl}_2$, $\text{H}_2\text{O}\text{-MgCl}_2$, $\text{H}_2\text{O}\text{-FeCl}_2$ and $\text{H}_2\text{O}\text{-LiCl}$ mixtures. The hydrate Raman spectra obtained from these inclusions include hydrohalite ($\text{NaCl}\cdot 2\text{H}_2\text{O}$), antarctite ($\text{CaCl}_2\cdot 6\text{H}_2\text{O}$), $\alpha\text{-CaCl}_2\cdot 4\text{H}_2\text{O}$, $\gamma\text{-CaCl}_2\cdot 4\text{H}_2\text{O}$, sinjarite ($\text{CaCl}_2\cdot 2\text{H}_2\text{O}$), $\text{FeCl}_2\cdot 6\text{H}_2\text{O}$, $\text{FeCl}_2\cdot 4\text{H}_2\text{O}$, and a LiCl hydrate. These spectra can be used as reference spectra for the analyses of natural fluid inclusions. The morphological variation of these spectra is dependent on temperature and relative orientation of the hydrate crystals if a polarized laser is used. However, these variations are only in peak intensities and not in peak positions, and thereby reliable parameters have been established for the identification of specific hydrate phases. The Raman spectra of mechanical mixtures in multi-component systems can be reconstructed by a simple addition of individual spectra according to their relative proportions.

Acknowledgements

This research is funded by the Austrian Science Fund (FWF, P18209-B06). The authors are grateful to I-Ming Chou, J. Fein, and an anonymous reviewer for their helpful comments.

References

- Bakker, R.J., 2004. Raman spectra of fluid and crystal mixtures in the system H_2O , $\text{H}_2\text{O}\text{-NaCl}$ and $\text{H}_2\text{O}\text{-MgCl}_2$ at low temperatures: applications to fluid inclusion research. *Can. Mineral.* 42, 1283–1314.
- Banks, D.A., Yardley, B.W.D., 1992. Crush-leach analysis of fluid inclusions in small natural and synthetic samples. *Geochim. Cosmochim. Acta* 56, 245–248.
- Baumgartner, M., 2009. Analysis of salt-bearing aqueous solutions in synthetic fluid inclusions by microthermometry and cryogenic Raman spectroscopy. Ph.D. Thesis, University of Leoben, 157 pp.
- Baumgartner, M., Bakker, R.J., 2009. CaCl_2 -hydrate nucleation in synthetic fluid inclusions. *Chem. Geol.* 265, 335–344.
- Borisenko, A.S., 1977. Study of the salt composition of solutions of gas–liquid inclusions in minerals by the cryometric method. *Geol. Geofiz* 18 (8), 16–27.
- Cathelineau, M., Marignac, C., Boiron, M.-C., Gianelli, G., Puxeddu, M., 1994. Evidence for Li-rich brines and early magmatic-rock interaction in the Larderello geothermal system. *Geochim. Cosmochim. Acta* 58, 1083–1099.
- Davis, D.W., Lowenstein, T.K., Spencer, R.J., 1990. Melting behaviour of fluid inclusions in laboratory-grown halite crystals in the systems $\text{NaCl}\text{-H}_2\text{O}$, $\text{NaCl}\text{-KCl}\text{-H}_2\text{O}$, $\text{NaCl}\text{-MgCl}_2\text{-H}_2\text{O}$, and $\text{NaCl}\text{-CaCl}_2\text{-H}_2\text{O}$. *Geochim. Cosmochim. Acta* 54, 591–601.

- Derome, D., Cathelineau, M., Fabre, C., Boiron, M.-C., Banks, D., Lhomme, T., Cuney, M., 2007. Paleo-fluid composition determined from individual fluid inclusions by Raman and LIBS: application to mid-proterozoic evaporitic Na–Ca brines (Alligator Rivers Uranium Field, northern territories, Australia). *Chem. Geol.* 237, 240–254.
- Dubessy, J., Audeoud, D., Wilkins, R., Kosztolanyi, C., 1982. The use of the Raman microprobe MOLE in the determination of the electrolytes dissolved in the aqueous phase of fluid inclusions. *Chem. Geol.* 37, 137–150.
- Dubessy, J., Boiron, M.-C., Moissette, A., Monnin, C., Sretenskaya, N., 1992. Determinations of water, hydrates and pH in fluid inclusions by micro-Raman spectroscopy. *Eur. J. Mineral.* 4, 885–894.
- Franks, F., 1972. Water, a Comprehensive Treatise. Volume 1. The Physics and Physical Chemistry of Water. Plenum Press. New York, N.Y. pp. 577.
- Franks, F., 1973. Water, a Comprehensive Treatise. Volume 2. Water in Crystalline Hydrates; Aqueous Solutions of Simple Nonelectrolytes. Plenum Press. New York, N.Y. pp. 661.
- Garg, A.K., 1988. High-pressure Raman-spectroscopic study of the ice 1 h – ice IX phase transition. *Phys. Status Solidi (a) - Appl. Res.* 110, 467–480.
- Gasparrini, M., Bakker, R.J., Bechstädt, T., 2006. Characterization of dolomitizing fluids in the carboniferous of the Cantabrian zone (NW Spain): a fluid-inclusion study with cryo-Raman spectroscopy. *J. Sed. Res.* 79, 1304–1322.
- Haynes, F., 1985. Determination of fluid inclusion composition by sequential freezing. *Econ. Geol.* 80, 1436–1439.
- Heinrich, C.A., Pettke, T., Halter, W.E., Aigner-Torres, M., Audetat, A., Gunther, D., Hattendorf, B., Bleiner, D., Guillong, M., Horn, I., 2003. Quantitative multi-element analysis of minerals, fluid and melt inclusions by laser-ablation inductively-coupled-plasma mass-spectrometry. *Geochim. Cosmochim. Acta* 67, 3473–3497.
- Linke, W.F., 1958. Solubilities: Inorganic and Metal-Organic Compounds. Volume I. American Chemical Society, Washington DC. 1440 pp.
- Manewa, M., Fritz, H.P., 1972. Schwingungsspektroskopische Untersuchungen der Hydrate des LiCl. *Z. Anorg. Allg. Chemie* 392, 227–235.
- Ni, P., Ding, J., Rao, B., 2006. In situ cryogenic Raman spectroscopic studies on the synthetic fluid inclusions in the systems H₂O and NaCl–H₂O. *Chin. Sci. Bull.* 51, 108–114.
- Roedder, E., 1984. Fluid inclusions. : *Rev. Mineral.*, 12. Mineralogical Society of America, p. 646.
- Samson, I.M., Walker, R.T., 2000. Cryogenic Raman spectroscopic studies in the system NaCl–CaCl₂–H₂O and implications for low-temperature phase behaviour in aqueous fluid inclusions. *Can. Mineral.* 38, 35–43.
- Schiffries, C.M., 1990. Liquid-absent aqueous fluid inclusions and phase equilibria in the system CaCl₂–NaCl–H₂O. *Geochim. Cosmochim. Acta* 54, 611–619.
- Schneider, J., Bakker, R.J., Bechstädt, T., Littke, R., 2008. Fluid evolution during burial diagenesis and subsequent orogenic uplift: the La Vid Group (Cantabrian Zone, Northern Spain). *J. Sed. Res.* 78, 282–300.
- Yardley, B.W.D., Graham, J.T., 2002. The origins of salinity in metamorphic fluids. *Geofluids* 2, 249–256.
- Zwart, E.W., Touret, L.R., 1994. Melting behaviour and composition of aqueous fluid inclusions in fluorite and calcite: applications within the system H₂O–CaCl₂–NaCl. *E. J. Mineral.* 6, 773–786.